Preparation of Zr-Containing Layered Double Hydroxides and Characterization of the Acido-Basic Properties of Their Mixed Oxides

Didier Tichit,* Nigamananda Das,† Bernard Coq, and Robert Durand

Laboratoire de Matériaux Catalytiques et Catalyse en Chimie Organique, UMR 5618 CNRS/ENSCM 8, rue Ecole Normale, 34296 Montpellier Cedex 5, France

Received May 17, 2001. Revised Manuscript Received January 22, 2002

Multicomponent M(II)/Al/Zr layered double hydroxides (LDHs) with M(II) = Mg, Ni, and Zn, exhibiting single hydrotalcite-like phases by XRD, were obtained by coprecipitation at constant pH = 10. The cationic contents were close to those of the solutions, excepted for Zr, for which 95, 70, and 65 mol % of the amount in solution were introduced in the Mg-, Ni-, and Zn-containing LDHs, respectively. This suggests either an easier accommodation of Zr when the size of the divalent cation decreases or a different behavior of the solutions during precipitation at pH 10. The introduction of Zr^{4+} of high ionic size induces a distortion of the brucite-like sheets and a heterogeneous distribution of charges, as evidenced by a lowering of the symmetry of the intercalated species. The lattice *a* parameter follows the Vegard correlation as a function of the (Al + Zr)/[M(II) + Al + Zr] ratio when M(II) = Mg and Ni, but it is nearly constant in Zn-containing LDHs for varying (Al + Zr)/(Zn + Al + Zr). This suggests, in these latter samples, the formation of pure lamellar phases with similar (Al + Zr)/(Zn + Al + Zr) ratios, regardless of the composition in solution, with an additional Zn-containing phase. At the same time, the presence of an excess of carbon in these samples, in addition to the compensating CO_3^{2-} species belonging to the layer structure, suggests that hydrozincite $Zn_5(CO_3)_2(OH)_6$ is the excedent phase. The introduction of Zr in the layers increases the basicity of the poorly basic Zn-containing mixed oxides but not the basicity of the Zn-containing LDHs. The basicity of the lamellar structure decreases as a result of the lowering of the partial charge of the oxygen atoms, whereas that of the mixed oxide increases through the formation of $Zr^{4+}-O^{2-}$ acid−base pairs.

Introduction

Layered double hydroxides (LDHs) constitute a class of compounds with positively charged layers and exchangeable anions in the interlayer space. Their general formula can be written $[M^{2+}_{1-x}M^{3+}_x(OH)_2][A^{n-}_{x/n}]\cdot mH_2O$, with divalent and trivalent cations in the layers. The structure is similar to that of brucite $Mg(OH)_2$, where Mg^{2+}-centered octahedra are linked by their edges to form infinite sheets. In the natural mineral hydrotalcite, whose name has been extended to this family of materials, some Mg^{2+} ions are replaced isomorphously by Al^{3+}, and the formal positive charge in the hydroxyl layers is usually compensated by carbonates.[1−3] These materials have already been used as anionic exchangers and as precursors of catalysts with basic sites and redox properties when reducible cations are introduced in the layers.[2,3] Structures containing noble metal cations have been reported recently that offer interesting opportunities as precursors of supported metal catalysts.[4,5] This emphasizes the role played by the cationic composition of LDHs for control of the properties of the mixed oxides obtained after thermal treatments. As a result, LDH structures with a wide variety of mono- to tetravalent cations have been gaining increasing interest.[5−15] On that account, the introduction of tetravalent cations, which greatly modifies the layer charge, could be an attractive route for the generation of unusual acido-basic properties. Velu et al.[15] have recently described the synthesis of Mg/Al/Zr LDHs tested as catalysts in the hydroxylation of phenol using H_2O_2 as the oxidant.

* To whom correspondence should be addressed. E-mail: tichit@cit.enscm.fr.

† Present address: National Metallurgical Laboratory, Jamshedpur 831007, India.

(1) Reichle, W. T. *CHEMTECH* **1986**, *16*, 58.
(2) Cavani, F.; Trifiro, F.; Vaccari, A. *Catal. Today* **1991**, *11*, 2.
(3) Vaccari, A. *Appl. Clay Sci*. **1999**, *14*, 161.
(4) Basile, L.; Basini, L.; Fornasari, G.; Trifiro, F.; Vaccari, A. *J. Chem. Soc., Chem. Commun*. **1996**, 2435.
(5) Basile, F.; Fornasari, G.; Gazzano, M.; Vaccari, A. *Appl. Clay Sci*. **2000**, *16*, 185.
(6) Serna, C. J.; Rendon, J. L.; Iglesias, J. E. *Clays Clay Miner*. **1982**, *30*, 180.
(7) Tichit, D.; Ribet, S.; Coq, B. *Eur. J. Inorg. Chem*. **2001**, 539.
(8) Coq, B.; Tichit, D.; Ribet, S. *J. Catal*. **2000**, *189*, 117.
(9) Rives, V.; Labajos, F. M.; Trujillano, R.; Romeo, E.; Royo, C.; Monzon, A. *Appl. Clay Sci*. **1998**, *13*, 363.
(10) Monzon, A.; Romeo, E.; Royo, C.; Trujillano, R.; Labajos, F. M.; Rives, V. *Appl. Catal. A: Gen*. **1999**, *185*, 53.
(11) Auer, S. M.; Grunwaldt, J. D.; Köppel, R. A.; Baiker, A. *J. Mol. Catal. A: Chem*. **1999**, *139*, 305.
(12) Labajos, F. M.; Rives, V.; Malet, P.; Centeno, M. A.; Ulibarri, M. A. *Inorg. Chem*. **1996**, *35*, 1154.
(13) Fernandez, J. M.; Barriga, C.; Ulibarri, M. A.; Labajos, F. M.; Rives, V. *Chem. Mater*. **1997**, *9*, 312.
(14) Ulibarri, M. A.; Hernandez, M. J.; Cornejo, J.; Serna, C. *J. Mater. Chem. Phys*. **1986**, *14*, 569.
(15) Velu, S.; Ramaswamy, Y.; Ramani, A.; Chanda, B. M.; Sivasanker, S. *Chem. Commun*. **1997**, 2107.

10.1021/cm011125l CCC: $22.00
Published on Web 03/27/2002

Table 1. Chemical Compositions of the Synthesis Solutions and the Solids and Some Morphological Features of the LDH Samples

	chemical composition (g/100 g)				M(II)/Al/Zr		(Al + Zr)/[M(II) + Al + Zr]					
sample	M(II)	Al	Zr	C	solution	solid	solution	solid	$2CO_3^{2-}/(Al^{3+} + 2Zr^{4+})$	*a* (nm)[a]	*a* (nm)[b]	specific surface area[c] ($m^2\ g^{-1}$)
Mg3	21.56	9.14		2.56	3/1/0	2.9/1.1/0	0.25	0.28	1.26	0.3050	0.3049	237
Mg3Zr0.3	20.92	7.35	7.60	2.50	3/0.7/0.3	2.84/0.88/0.27	0.25	0.29	0.95	0.3043	0.3049	201
Mg2.6Zr0.32	18.09	8.80	6.92	2.98	2.64/1/0.32	2.6/1.14/0.26	0.33	0.35	1.05	0.3023	0.3038	252
Ni3	40.29	6.79		1.74	3/1/0	2.9/1.1/0	0.25	0.27	1.15	0.3036	–	203
Ni3Zr0.3	39.98	4.32	4.33	1.88	3/0.7/0.3	3.06/0.72/0.21	0.25	0.23	1.21	0.3049	–	218
Zn3	44.09	6.05		2.37	3/1/0	3/1/0	0.25	0.25	1.76	0.3072	0.3056	91
Zn3Zr0.1	43.89	5.40	1.54	2.60	3/0.9/0.1	3/0.9/0.076	0.25	0.25	1.88	0.3069		121
Zn3Zr0.3	43.23	4.15	4.05	2.93	3/0.7/0.3	3.08/0.7/0.20	0.25	0.23	2.07	0.3063	0.3063	127
Zn2.6Zr0.32	35.83	6.06	4.98	2.25	2.64/1/0.32	2.66/1.1/0.27	0.33	0.34	1.19	0.3076	0.3061	116

[a] As-prepared sample. [b] Sample calcined at 620 K and rehydrated. [c] Sample calcined at 720 K.

However, the acido-basicity of the samples was not extensively studied. This prompted us to prepare M(II)/Al/Zr LDHs with M(II) = Zn, Mg, and Ni, on one hand, to compare the structural modifications induced by the introduction of Zr into the most largely studied hydrotalcite-like structures (Mg/Al, Ni/Al, Zn/Al) and, on the other hand, to investigate the acido-basicity of their mixed oxides in view of catalytic applications.

Experimental Section

Methods. Chemical analyses of the as-prepared solids were performed at the Service Central d'Analyse du C.N.R.S. (Solaize, France) by ICP-MS.

XRD powder patterns were collected on a CGR Theta 60 instrument (40 kV, 20 mA) using monochromatized Cu $K\alpha_1$ radiation (λ = 0.15401 nm, 40 kV, 50 mA) on samples as-prepared or treated as follows: LDHs were calcined at 723 K for 4 h with synthetic air flow (100 $cm^3\ min^{-1}$, ramp = 1 K min^{-1}).

BET specific surface areas were determined by N_2 adsorption at 77 K with a Micromeritics ASAP 2000 apparatus on samples calcined at 723 K and outgassed at 523 K and 10^{-4} Pa.

Diffuse reflectance FTIR spectra of the powdered samples were recorded on a Bruker Equinox 55 FTIR spectrometer supplied with a MCT detector and a diffuse reflectance attachment. An infrared cell of dome shape (Craseby-Specac) with a ZnSe window was used under a flow of air (10 $cm^3\ min^{-1}$).

TG experiments were carried out in a Setaram TG-DSC-111 apparatus, with fully programmable heating and cooling sequences, sweep gas valve switchings, and data analysis. About 50 mg of an as-prepared sample were placed in a platinum crucible and dried at 393 K in He (flow = 20 $cm^3\ min^{-1}$). Thermal analysis was performed from room temperature to 873 K in a He stream (flow = 20 $cm^3\ min^{-1}$, ramp = 1 K min^{-1}). The composition of gas outflowing the TG-DSC apparatus was monitored continuously on-line with a Leybold Transpector SQX quadrupole mass spectrometer (0−200 amu) following masses 18 (H_2O) and 44 (CO_2).

The basicity of the calcined samples was studied by the adsorption and temperature-programmed desorption (TPD) of CO_2 with a Setaram TG-DSC-111 microcalorimeter. The samples were previously outgassed at 723 K, cooled to 373 K, and contacted with flowing CO_2. After the thermal events had been recorded under isothermal conditions, weakly adsorbed CO_2 was removed in a He flow at 373 K, and TPD experiments were then performed following the weight loss under He flow from 373 to 723 K (ramp = 10 K min^{-1}) and the nature of outflowing gas by MS coupling.

The total acidity of the calcined samples was studied by NH_3 adsorption and TPD experiments using a conductivity cell for the detection of the effluent gases. The samples were previously outgassed at 723 K, then cooled at 373 K, and contacted with NH_3 vapor. After the sample was purged, the temperature was increased to 723 K (ramp = 10 K min^{-1}); the evolved ammonia was trapped in a HCl solution and finally titrated.

Materials Preparation. The materials were synthesized by coprecipitation at room temperature under air. For the syntheses, 250 cm^3 of a solution containing the appropriate concentrations of magnesium (nickel or zinc) and aluminum nitrates and zirconium oxynitrates salts (Aldrich) was delivered into a polypropylene reactor by a chromatography-type pump at a constant flow of 1 $cm^3\ min^{-1}$. A second aqueous solution of 2 M NaOH and 0.5 M Na_2CO_3 was simultaneously fed by a pH-stat apparatus (718 Stat Titrino, Metrohm). The careful control of the flow maintained the pH in the reactor during precipitation at a constant value of ca. 10.0 ± 0.2. After the precipitation was complete, the resulting suspension was aged at 353 ± 5 K for 15 h with stirring. The solid was then isolated by centrifugation, washed thoroughly with deionized water, and dried overnight at 353 K in an oven.

Samples with nominal contents in cations of M(II)/Al/Zr = 3/1/0 and 3/0.7/0.3 [M(II) = Mg, Ni], M(II)/Al/Zr = 3/0.9/0.1 [M(II) = Zn], and M(II)/Al/Zr = 2.64/1/0.32 [M(II) = Mg, Zn] were synthesized. Samples will hereafter be referred to as M*x*Z*ry*, where *x* and *y* are the molar fractions in solution of M(II) and Zr, respectively.

Results

Characterization of the As-Prepared Samples. The compositions of the precipitated samples are compared to those of the solutions in Table 1. The only remarkable discrepancy is that the amount of Zr is always slightly lower in the solids than in the solutions. Comparing Mg3Zr0.3, Ni3Zr0.3, and Zn3Zr0.3, which had the same cationic contents in solutions, the amount of Zr incorporated into the solids increases according to the divalent cation in the order Zn ≈ Ni < Mg. The (Al + Zr)/[M(II) + Al + Zr] ratio is higher than expected in Mg-containing LDHs, whereas the ratios are similar in the solutions and solids for Zn-containing ones. For Ni-containing samples, this ratio decreases significantly when Zr is introduced. These results reflect specific behaviors of the different cationic mixtures during precipitation. The ratio $2CO_3^{2-}/(Al^{3+} + 2Zr^{4+})$ between the total amounts of negative and positive charges must be unity in the hydrotalcite-like structures (Table 1). This rarely occurs as, except for Mg3Zr0.3, a systematic excess of negative charge is obtained. It reaches 25% in Mg- and Ni-containing LDHs, and up to 100% in Zn-containing ones. This could be due to bicarbonate species formed during washing steps,[16] which leads to an overestimation of the anionic charge if expressed as

(16) Del Arco, M.; Rives, V.; Trujillano, R.; Malet, P. *J. Mater. Chem.* **1996**, *6*, 1419.

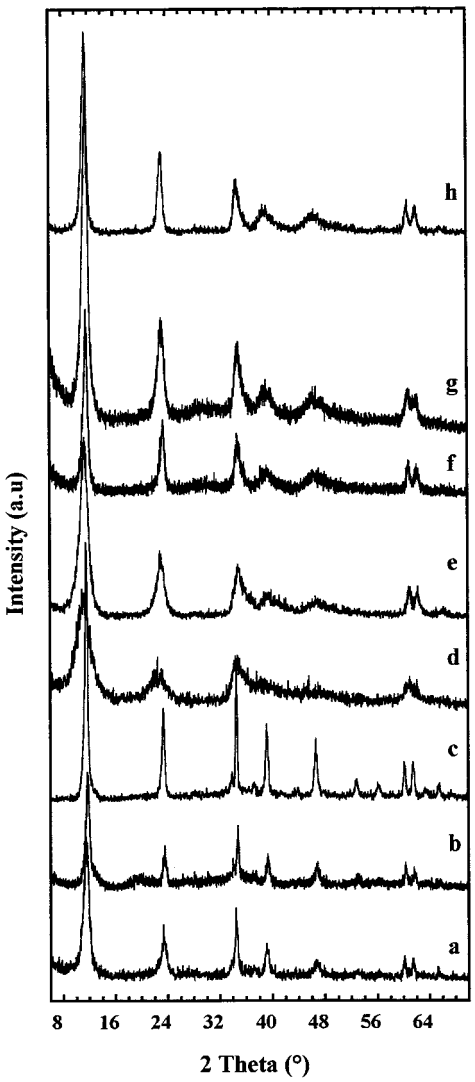

Figure 1. XRD patterns of (a) Zn2.6Zr0.32, (b) Zn3Zr0.3, (c) Zn3, (d) Ni3Zr0.3, (e) Ni3, (f) Mg2.6Zr0.3, (g) Mg3Zr0.32, and (h) Mg3.

CO_3^{2-}. Nevertheless, the net excess of negative charge found for Zn-containing samples likely implies that, in addition to the hydrotalcite-like phase, an additional carbonate phase could be formed.

XRD powder patterns of the dried samples show a single hydrotalcite-like phase in all cases (Figure 1). The crystallinity slightly decreases in Zr-containing samples. The mean crystallite sizes determined with the Scherrer equation increase from 3.5−5.5 to 7.5 and 8.5−10 nm on going from Ni- to Mg- and Zn-containing LDHs, respectively.

The lattice *a* parameters, related to *d*(110) according to $a = 2 \times d(110)$, are in the range of 0.3036−0.3072 nm for Zr-free samples, which is consistent with literature data for such samples when the Al/[M(II) + Al] ratios are in the range of 0.22−0.33 (Table 1).[17−19] Substitution of Zr^{4+}, which has a larger ionic radius (0.072 nm), for Al^{3+} (0.053 nm) is expected to increase the lattice *a* parameter. This is not the case, although

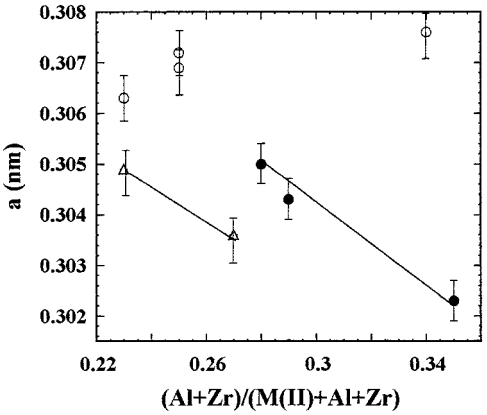

Figure 2. Variation of the lattice *a* parameter of the (●) Mg-, (△) Ni-, and (○) Zn-containing samples as a function of the (Al + Zr)/[M(II) + Al + Zr] ratio.

an increase in the lattice *a* parameter with increasing Zr^{4+} content was reported by Velu et al.[15] However, this was for a series of Mg/Al/Zr LDHs with similar (Al + Zr)/(Mg + Al + Zr) ratios, in contrast to our samples in which this ratio varies greatly. As shown in Figure 2, the lattice *a* parameter decreases with decreasing M(II) (Mg or Ni) in (Al + Zr)/[M(II) + Al + Zr], thus following the Vegard correlation. This shows that the thickness of these brucite-like layers is weakly influenced by the substitution of Zr for Al at amounts lower than 20 mol %. In contrast, the lattice *a* parameter does not vary significantly for different (Al + Zr)/(Zn + Al + Zr) ratios and has a mean value of ca. 0.3070 nm. This suggests that, regardless of the composition in solution, a lamellar phase is formed in these solids with always the same (Al + Zr)/(Zn + Al + Zr) molar ratio.

TG diagrams of the samples have very similar shapes, as shown in Figure 3, with total weight losses at 870 K ranging from 25 to 43% (Table 2). Major losses of mass occur mainly in two steps. The first is due to the elimination of physically adsorbed and interlayer water molecules, whereas the second is due to dehydroxylation of the layers and loss of the anions. The second weight loss is definitely smaller in Zn-containing LDHs. Furthermore, a third mass loss of ca. 2−3 wt % is also observed in these samples as a broad endothermic event between 720 and 870 K that can barely be detected in the heat flow profiles. The first endothermic peak in the heat flow profile is within the range 390−470 K for all samples, whereas the second peak is within the range 550−690 K in Mg- and Ni-containing samples and within the range 490−520 K in Zn-containing ones. Mass spectrometry (MS) analyses of outflowing gases show that H_2O and CO_2 are present in both domains (Figure 4). In the low-temperature range, the weight loss corresponds to the release of weakly bonded species, and in the high-temperature range, it corresponds to dehydroxylation and decomposition of compensating anions. Several well-defined maxima are associated with the latter, showing that several carbonate species are formed. Dehydroxylation and decarbonation occur concurrently. These behaviors are in agreement with those generally reported for LDHs.[20−22] The first weight loss was used to determine the amounts of intercalated

(17) Thevenot, F.; Szymanski, R.; Chaumette, P. *Clays Clay Miner.* **1989**, *37*, 396.
(18) Kooli, F.; Depège, C.; Ennaqadi, A.; De Roy, A.; Besse, J. P. *Clays Clay Miner.* **1997**, *45*, 92.
(19) Miyata, S. *Clays Clay Miner.* **1975**, *23*, 369.
(20) Rey, F.; Fornés, V.; Rojo, J. M. *J. Chem. Soc., Faraday Trans.* **1992**, *88*, 2233.

Table 2. Data from TG-DSC Experiments for CO_2 Adsorption and from TPD of NH_3 on the Various Samples

	TG analysis								
	first peak		second peak			CO_2 adsorption		NH_3 adsorption	
sample	weight loss (%)	T (K)	weight loss (%)	T (K)	total weight loss (%)	ΔH (kJ mol^{-1})	Nb[a] $\times 10^3$ (mequiv/m^2)	T_M[b] (K)	Na[c] $\times 10^3$ (mequiv/m^2)
Mg3	15	480	28	690	43	76	5.95		0.67
Mg3Zr0.3	16.4	450	23.6	650	40	75	7.06	515	1.24
Mg2.6Zr0.32	14.2	470	22.8	610	37	72	5.12	520	0.67
Ni3	15	440	19	580	34	66	2.71		
Ni3Zr0.3	12	390	20	550	32	72	1.51		
Zn3	12.7	425	12.3	520	25	48	0.66	510	2.20
Zn3Zr0.1	15.4	420	12.6	490	28	72	0.99		
Zn3Zr0.3	11.6	425	14.4	490	26	54	1.02	510	2.05
Zn2.6Zr0.32						19	0.52		

[a] Number of basic sites. [b] Temperature of maximum rate of desorption of NH_3. [c] Number of acid sites.

Table 3. Chemical Compositions of the Samples and of the Suggested Mixtures of Zn-LDHs and Hydrozincite

sample	phases	HDL + hydrozincite
Mg3	$[Mg_{0.73}Al_{0.27}(OH)_2](CO_3)_{0.17}\cdot 0.92H_2O$	
Mg3Zr0.3	$[Mg_{0.71}Al_{0.22}Zr_{0.068}(OH)_2]](CO_3)_{0.17}\cdot 0.8H_2O$	
Mg2.6Zr0.32	$[Mg_{0.65}Al_{0.28}Zr_{0.066}(OH)_2](CO_3)_{0.215}\cdot 0.7H_2O$	
Ni_3	$[Ni_{0.73}Al_{0.27}(OH)_2]\ (CO_3)_{0.155}\cdot 0.83H_2O$	
$Ni_3Zr_{0.3}$	$[Ni_{0.77}Al_{0.18}Zr_{0.054}(OH)_2](CO_3)_{0.177}\cdot 0.74H_2O$	
Zn3	$[Zn_{0.77}Al_{0.25}(OH)_2](CO_3)_{0.22}\cdot 0.83H_2O$	$[Zn_{0.46}Al_{0.22}(OH)_2](CO_3)_{0.112}\cdot 0.83H_2O + 0.043[Zn_5(CO_3)_2(OH)_6]$
Zn3Zr0.1	$[Zn_{0.757}Al_{0.224}\,Zr_{0.019}(OH)_2](CO_3)_{0.243}\cdot 0.9H_2O$	$[Zn_{0.477}Al_{0.224}Zr_{0.019}(OH)_2](CO_3)_{0.112}\cdot 0.9H_2O + 0.056[Zn_5(CO_3)_2(OH)_6]$
Zn3Zr0.3	$[Zn_{0.77}Al_{0.178}\,Zr_{0.051}(OH)_2](CO_3)_{0.282}\cdot 0.8H_2O$	$[Zn_{0.415}Al_{0.178}Zr_{0.051}(OH)_2](CO_3)_{0.14}\cdot 0.8H_2O + 0.071[Zn_5(CO_3)_2(OH)_6]$
Zn2.6Zr0.32	$[Zn_{0.664}Al_{0.27}\,Zr_{0.066}(OH)_2](CO_3)_{0.226}\cdot m H_2O$	$[Zn_{0.539}Al_{0.27}Zr_{0.066}(OH)_2](CO_3)_{0.2}\cdot m H_2O + 0.025[Zn_5(CO_3)_2(OH)_6]$

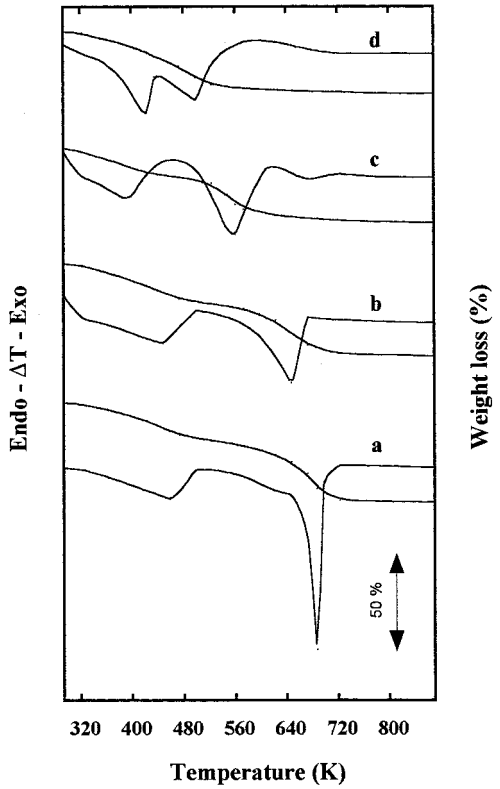

Figure 3. TG analysis and heat flow profiles of various samples: (a) Mg3, (b) Mg3Zr0.3, (c) Ni3Zr0.3, and (d) Zn3Zr0.3.

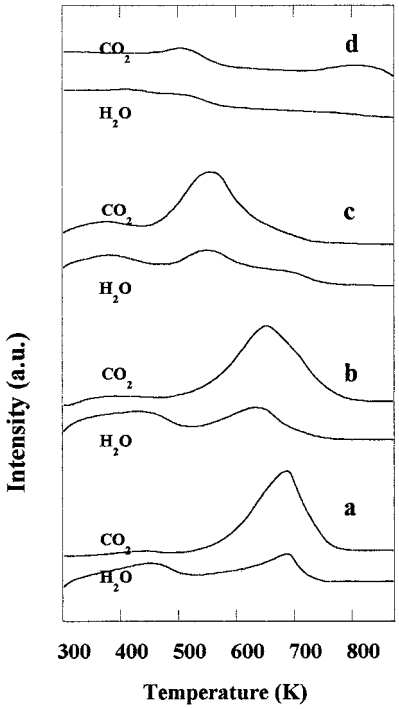

Figure 4. Temperature-programmed decomposition followed by mass spectrometry of (a) Mg3, (b) Mg3Zr0.3, (c) Ni3Zr0.3, and (d) Zn3Zr0.3.

water, given in the LDH formula (Table 3), neglecting the very small amount of CO_2 also released. The temperature maximum of the second peak in the heat flow profile is shifted toward higher temperatures on going from Zn- to Ni- and Mg-containing samples, reflecting the concurrent increase of basicity; the bonding energies of carbonates are indeed related to the basic strengths of the solids.[23] Moreover, this second endotherm profile becomes broader and shifts back to lower temperatures when Zr is introduced in Mg- and Ni-LDHs. MS profiles of Zr-containing samples in the temperature range of the second heat flow peak show a broad peak of CO_2 evolution shifted toward lower

(21) Bellotto, M.; Rebours, B.; Clause, O.; Lynch, J.; Bazin, D.; Elkaïm, E. *J. Phys. Chem.* **1996**, *100*, 8535.
(22) Hibino, T.; Yamashita, Y.; Kosuge, K.; Tsunashima, A. *Clays Clay Miner.* **1995**, *43*, 427.
(23) Sanchez Valente, J.; Figueras, F.; Gravelle, M.; Kumbhar, P.; Lopez, J.; Besse, J. P. *J. Catal.* **2000**, *189*, 370.

temperature when compared to that of the Zr-free samples. H_2O is simultaneously released. This shows that dehydroxylation and decarbonation are both shifted toward lower temperature when Zr is present. MS analysis shows that a weak amount of CO_2 evolves between 720 and 870 K in Zn-containing samples, therefore giving rise to the endotherm previously detected and pointing out the likely occurrence of an additional carbonate phase.

Characterization of Layered Double Hydroxides upon Thermal Treatment. Decomposition of the LDH structure was followed by recording IR spectra of the samples at increasing temperature in steps of 50 K up to 723 K. These spectra are presented in Figures 5 and 6 for the Mg- and Zn-LDHs, respectively. Before activation (293 K), the IR bands with a maximum at 3464 cm^{-1} due to OH stretching of hydrogen-bonded hydroxyl groups and H_2O are skewed on the right-hand side and have a net shoulder at 3060 cm^{-1} due to hydrogen bonding between H_2O and interlayer anions.[12,19] A second shoulder at 3576 cm^{-1} in Mg3, not observed in Zn3, suggests a second type of OH species with a highly basic character. This species could be hydroxyl groups in low-coordinated sites such as corners and edges. H_2O bending vibrations also give a band at 1646 cm^{-1}. The sharp and intense bands appearing at 1365 and 1379 $cm^{-1,}$ with shoulders at ca. 1506 and 1530 cm^{-1} for Zn- and Mg-containing samples, respectively, are assigned to symmetric and antisymmetric O−C−O stretching vibrations of monodentate carbonate species. The shifts from the normal position of the free carbonate species, i.e., 1450 cm^{-1}, and the splittings of about 150 cm^{-1} result from a lowering of the symmetry of the species in the interlayer domain. These shifts are higher than in LDHs containing cations with large ionic sizes such as Y, V, and Cr in Mg/Al/Y,[13] Ni/V,[24] or Zn/Cr[16] with values of 115, 116, and 126 cm^{-1}, respectively. These features could account for a greater distortion of the brucite-like layers and for a heterogeneous distribution of positive charge in the brucite-like layers containing cations of different charges when both Al^{3+} and Zr^{4+} are present. Accordingly, when the Zr content increases, the bands at high frequency exhibit a broadening, along with the appearance of several shoulders and an increase in intensity relative to their companion band. These facts indicate that carbonate species with different symmetries are formed. As the temperature of the treatment increases, a net decrease in intensity of the hydroxyl and H_2O bands is observed. Moreover, in Zn-containing samples, the dominating hydroxyl band shifts to 3533 cm^{-1} after treatment at 423 K, showing a lower extent of hydrogen bonding between OH groups, while the shoulder moves progressively from 3060 at room temperature to 2850 cm^{-1} at 473 K and the band at 1640 cm^{-1} disappears. Removal of the interlayer water and dehydroxylation of the layers is complete after treatment above 623 K, as shown by the complete vanishing of the related vibration bands. In Mg-containing LDHs, the hydroxyl band shifts to 3576 cm^{-1} after treatment at 573 K and remains quite intense at 723 K, providing evidence that these samples remain highly hydroxylated at this temperature. The shift from 3533 to 3576 cm^{-1} of the OH stretching mode of free hydroxyls from Zn- to Mg-containing LDHs treated at 573 K shows an increase in their basic strength.[25]

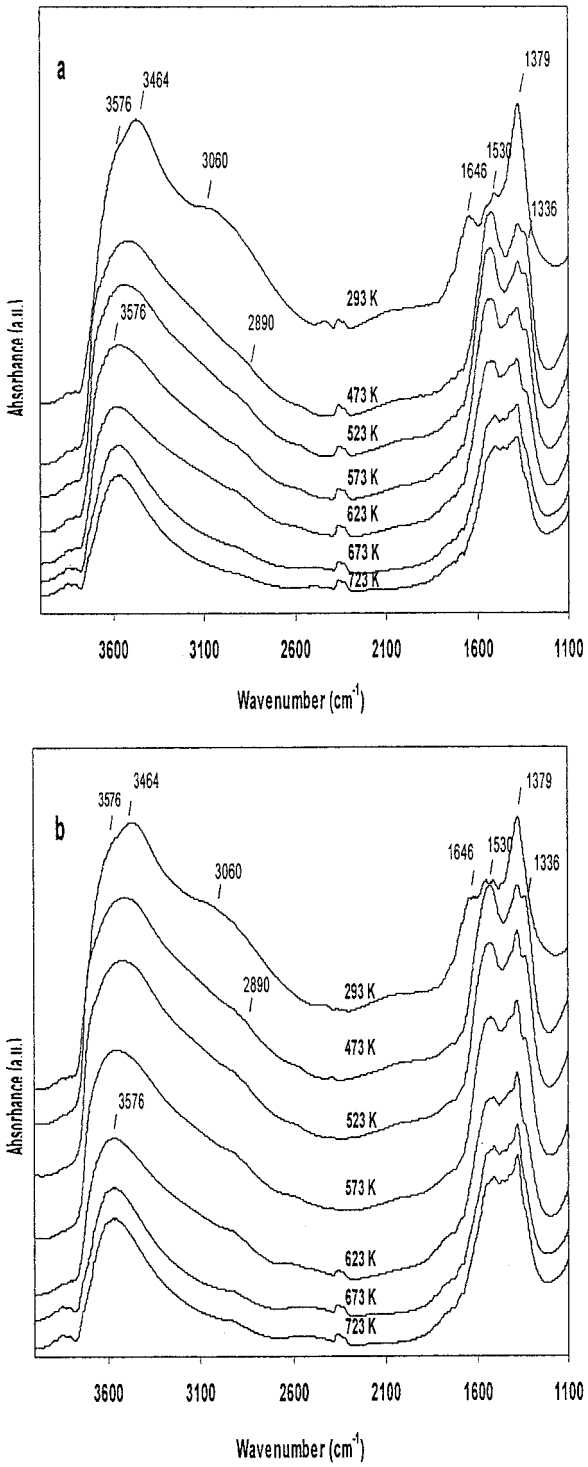

Figure 5. DRIFT spectra of (a) Mg3 and (b) Mg3Zr0.3 evacuated at increasing temperature.

The intensities of the carbonate bands also decrease as a result of progressive decarbonation during thermal treatment. It is worth noting that carbonates are still present in Mg- and Zn-containing samples after treatment at 723 K; however, they are in larger amounts in

(24) Labajos, F. M.; Sastre, M. D.; Trujillano, R.; Rives, V. *J. Mater. Chem*. **1999**, *9*, 1033.

(25) Prinetto, F.; Ghiotti, G.; Graffin, P.; Tichit, D. *Microporous Mesoporous Mater*. **2000**, *39*, 229.

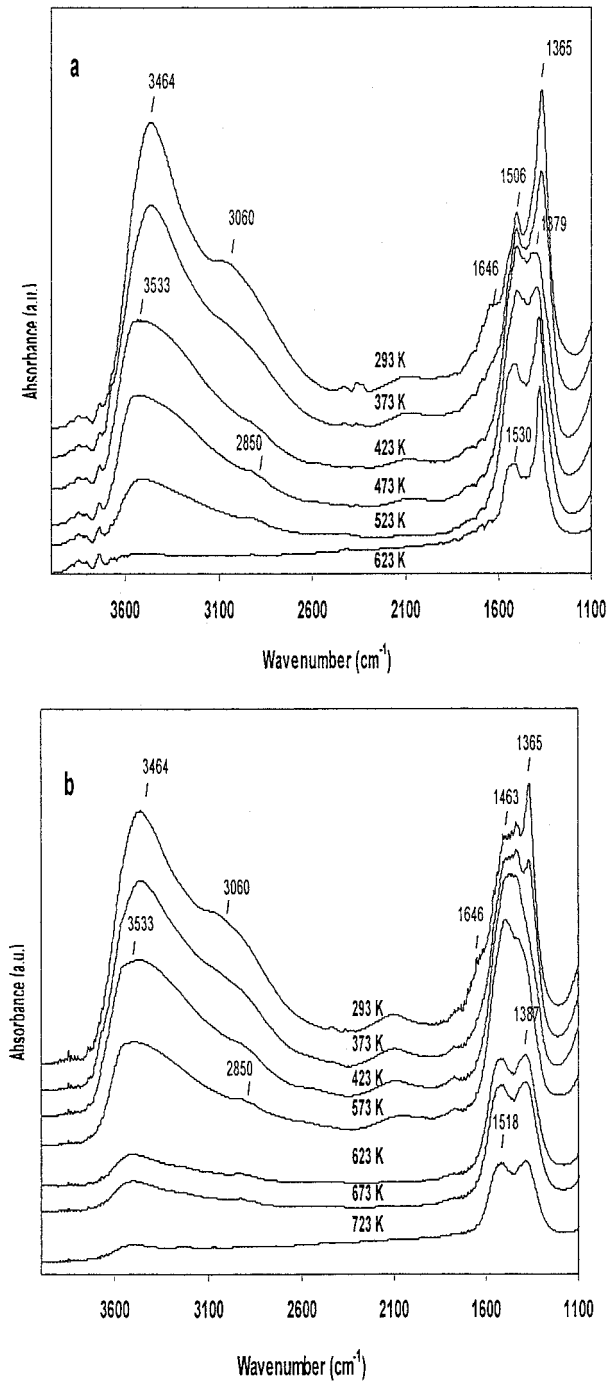

Figure 6. DRIFT spectra of (a) Zn3 and (b) Zn3Zr0.3 evacuated at increasing temperature.

the former because of the well-known higher basicity of these materials. No specific behavior is observed when Zr is present. The two peaks of the unidentate carbonate species exhibit similar intensities after treatment at 473 K, which indicates a change in the symmetry of these carbonates when interlayer water is removed at the same time, as shown by the simultaneous disappearance of the broad shoulder at 3060 cm^{-1}.

Note that weak carbonate bands are still present in Zn3 at 623 K, even though it is totally dehydroxylated, with a splitting of 150 cm^{-1} but with a net difference in intensity between the two peaks. This suggests a trapping of carbonate species in the decomposed material.

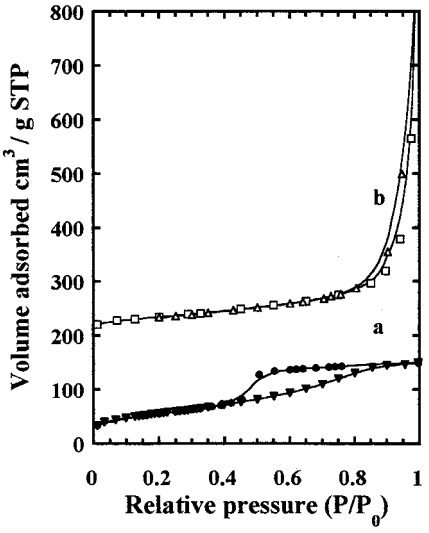

Figure 7. Nitrogen adsorption−desorption isotherms at 77 K of (a) Mg3Zr0.3 and (b) Zn3Zr0.3.

The XRD patterns of Mg3 and Mg3Zr0.3 calcined at 723 K are characteristics of a poorly crystallized MgO-like phase. The lattice *a* parameter in Mg3 slightly decreases, compared to that in pure MgO, as a result of the incorporation of Al cations in the lattice, as generally reported.[2,3,26] Conversely, the *a* parameter in Mg3Zr0.3 is the same as that in MgO, suggesting that Zr and Al are both introduced, leading to a compensating effect. Zn-containing LDHs calcined at 723 K also exhibit the mixed oxide Zn(Al)O structure with a lattice *a* parameter smaller than that found in pure ZnO, suggesting that Al alone or only trace amounts of Zr are incorporated into the structure. These results suggest that higher segregation of Zr occurs in ZnO than in MgO-like mixed oxides during calcination.

After calcination at 723 K, significant differences appear in the specific surface areas of the mixed oxides (Table 1). They are greater than 200 $m^2\ g^{-1}$ in Mg- and Ni-containing LDHs but reach only 120−130 $m^2\ g^{-1}$ in Zn-containing LDHs. One can note that Zr-containing Zn-LDHs have surface area values 30% higher than Zr-free samples. Moreover, the nitrogen adsorption−desorption isotherms exhibit very different shapes (Figure 7). Mg- and Ni-containing samples present type IV isotherms with H2 hysteresis loops, whereas straight H3 hysteresis loops above $P/P_0 \approx 0.9$ are found for Zn-containing LDHs. The latter are characteristic of clay minerals with N_2 physisorption between aggregates of platelet particles. These different behaviors show that the morphology of larger particles is very likely preserved upon calcination.

Rehydration of the Layered Double Hydroxides. Because of their so-called "memory effect", the original lamellar structures could be reconstructed by contact of the mixed oxides with solutions containing various anions.[3] However, depending on the nature of the cations involved, the total reconstruction requires different conditions. In the same way that the rehydration of nickel oxide to hydroxide is much more difficult than that of magnesium or zinc oxide,[27] the reconstruction of Ni/Al mixed oxides is less easy than that of Mg/Al

(26) Rebours, B.; d'Espinose de la Caillerie, J. P.; Clause, O. *J. Am. Chem. Soc.* **1994**, *116*, 1707.

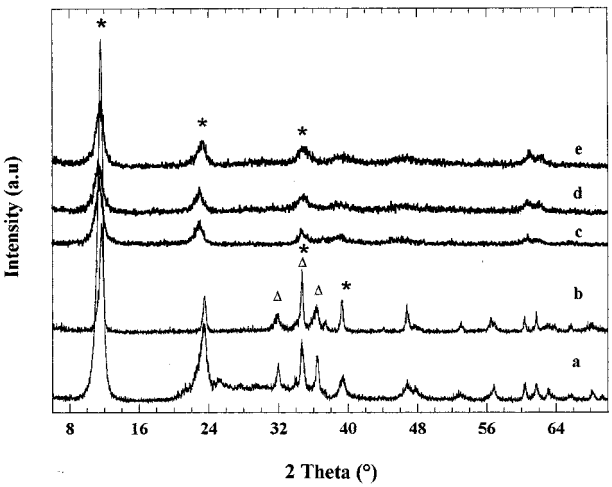

Figure 8. XRD patterns of the rehydrated materials: (a) Zn3, (b) ZnZr3, (c) Mg3, (d) Mg3Zr0.3, and (e) Mg2.6Zr0.32 (*, HDL; △, ZnO).

and Zn/Al mixed oxides. Moreover, in all cases, the ability to restore the lamellar structure also depends on the calcination temperature of the LDH precursor, which must remain lower than that required for the crystallization of spinel-like phases.[27] For temperatures below 873 K, LDH decomposition proceeds topotactically,[28] and restoration of the structure can occur. Reconstruction has been achieved under STP conditions for Mg/Al[29] and Zn/Al mixed oxides,[18] whereas treatments at 523 K and 4 MPa[26] or at 433 K and 0.6 MPa in the presence of NH_4OH[30] have been found necessary for the reconstruction of Ni/Al mixed oxides. To account for these features, the reconstruction of the different Mg- and Zn-type mixed oxides obtained after calcination at 723 K of the LDHs was investigated under ambient temperature and in contact with air for 5 h. The XRD patterns reported in Figure 8 show that the lamellar structures are fully reconstructed for the Mg-containing mixed oxides, as no difference could be identified between these patterns and those of their originals LDHs counterparts. Well-crystallized lamellar structures were also found in rehydrated Zn-containing compounds, although some extent of ZnO-like phase was still detected. The main compensating anions in reconstructed LDHs are CO_3^{2-} because of the presence of CO_2 in the surrounding atmosphere during the reconstruction process and the great affinity of CO_3^{2-} for LDH framework. The lattice *a* parameters of the lamellar structures were almost the same, having a mean value of 0.3060 nm, which is still very similar to the value in the original samples, This shows that similar (Zr + Al)/(Zn + Al + Zr) ratios are likely obtained in these structures, as suggested above.

Acido-Basicity of the Mixed Oxides. The strengths and number of basic sites of the mixed oxides were estimated by CO_2 adsorption followed by TG-DSC. The results are reported in Table 2. The enthalpy of CO_2 adsorption of the three types of LDHs decreases as follows according to the nature of divalent cation: Mg > Ni > Zn. Enthalpy values of about 80 and 70 kJ mol^{-1} for Mg- and Ni-containing LDHs, respectively, are consistent with previously reported data.[30,31] The same evolution appears for the density of sites in the three series of samples. However, larger differences are observed because, in Zn- and Ni-containing LDHs, the number of sites is 10 and 50%, respectively, of the number in Mg-containing LDHs. Upon the introduction of Zr, there is a slight increase of the enthalpy of CO_2 adsorption on Zn- and Ni-containing LDHs materials, which are of weak and medium basicity, but not in the case of Mg-containing LDHs, which are of strong basicity.

The numbers of acid sites, measured by NH_3 adsorption, are similar in Zn- and Mg-containing mixed oxides, thus showing the higher density of these acid sites in the former solid, which has a lower surface area. This underlines the stronger intrinsic basic character of Mg-containing samples, with 10-fold more basic than acid sites, and the reverse for Zn-containing samples.

Discussion

The materials investigated belong to the most extensively studied families of LDHs, i.e., the Mg- and Ni-containing LDHs corresponding to natural hydrotalcite and takovite minerals. Because of the stabilities of their lattices, a tetravalent cation such as Zr, with a large ionic radius (0.072 nm), can be accommodated to some extent in their layers. Multicomponent M(II)/Al/Zr LDHs [M(II) = Mg, Ni] were thus obtained and found to exhibit a pure lamellar structure. Their crystallinities decrease and the intensity ratios between their 003 and 006 peaks slightly increase, compared to Zr-free samples. These features can be attributed to a distortion of the layers when Zr is introduced. The thicknesses of their brucite-like layers are only slightly influenced by the substitution of Zr for Al. A similar result was reported by Basile et al.[5] when substituting Rh^{3+} for Al^{3+}. This can be explained by considering that the lattice *a* parameter is slightly affected by this type of substitution involving cations that are larger than Mg^{2+}, which predominates in the brucite-like layers. In contrast, the Zn-containing LDHs show a specific behavior. The (Al + Zr)/(Zn + Al + Zr) ratios of the solids correspond to those of the solutions (Table 1), but the quasi-invariance of the lattice *a* parameters with these ratios strongly suggests that the brucite-like layers of the different samples have similar compositions. Highly local ordering within the layers of the LDHs is obtained when trivalent cations are never neighboring each other. This condition is satisfied with M(II)/M(III) ratios of 0.25 and 0.33.[32] The latter value is commonly found in LDHs with different types of divalent and trivalent cations and particularly in natural minerals,[32,33] but specific behaviors have been reported by Thevenot et al.[17] for Zn/Al hydrotalcite-like compounds. In the range $0.26 \leq x = Al/(Zn + Al) \leq 0.65$, a pure lamellar phase was obtained

(27) Clause, O.; Rebours, B.; Merlen, E.; Trifiró, F.; Vaccari, A. *J. Catal.* **1992**, *133*, 231.
(28) Reichle, W. T.; Kang, S. Y.; Everhardt, D. S. *J. Catal.* **1986**, *101*, 352.
(29) Sato, T.; Kato, K.; Endo, T.; Shimada, M. *React. Solids* **1986**, *2*, 253.
(30) Prinetto, F.; Tichit, D.; Teissier, R.; Coq, B. *Catal. Today* **2000**, *55*, 103.
(31) Dumitriu, E.; Hulea, V.; Chelaru, C.; Catrinescu, C.; Tichit, D.; Durand, R. *Appl. Catal. A: Gen.* **1999**, *178*, 145.
(32) Brindley, G. W.; Kikkawa, S. *Am. Mineral.* **1979**, *64*, 836.
(33) Vucelic, M.; Jones, W.; Moggridge, G. D. *Clays Clay Miner.* **1997**, *45*, 803.

only for $x = 0.33$ and 0.37, whereas additional ZnO and bayerite phases were formed at lower and higher ratios, respectively. Moreover, in a study of the reconstruction of Zn/Al LDHs, Kooli et al.[18] always found a value of $Al/(Zn + Al) = 0.33$ in the rehydrated samples, irrespective of their initial composition. Last, Roussel et al.[34] reported that Zn/Cr/Cl LDHs could only be synthesized with the ratio $Cr/(Zn + Cr) = 0.33$ as a result of a cation ordering favored by the chromium cations.

In the samples of this study, one could speculate that the $(Al + Zr)/(Zn + Al + Zr)$ ratio is approximately 0.25 with the concurrent formation of an excedent Zn-containing phase. In this case, the ratio would indeed be close to that of the stable parent Zn/Al.[17,18] Because a large carbon excess was found in these samples, a zinc hydroxycarbonate phase, i.e., hydrozincite $Zn_5(CO_3)_2(OH)_6$, could be formed. The amounts formed in the different samples can be estimated from the carbon contents. One can consider that the layer charges result from the introduction of both Al and Zr cations into the structure, inducing one and two net positive charges, respectively, by the cation. These charges are compensated by CO_3^{2-}. The extent of carbon belonging to hydrozincite can therefore be calculated by subtracting from the total carbon content detected by chemical elemental analysis the amount attributed to charge-balancing CO_3^{2-} species in the interlayer space. The results concerning amount of hydrozincite calculated from the remaining carbon lead, in turn, to the calculation of the amount of Zn in the lamellar phase. The compositions of the latter and amounts of the former phases thus obtained are given in Table 3. They show that hydrozincite represents no more than 4−6 mol %, explaining why it was not detected by XRD. Significantly, LDH phases deduced from the previous calculations lead to $(Al + Zr)/(Zn + Al + Zr)$ ratios of ∼0.33. These results must obviously be carefully considered as they are based on arguments that suffer from several limitations such as the accuracy of carbon content measurements and the barely detectable presence in the XRD data of the hydrozincite phase.

The nature of the divalent cation has a clear influence on several other properties of the materials such as the specific surface area and basicity. The net decrease of the specific surface areas of Zn-containing samples as compared to those of Mg- or Ni-containing ones is in agreement with the higher crystallinity of the former samples, as well as with the higher carbonate contents of the Mg- and Ni-containing LDHs. A high carbonate content increases the specific surface area through the cratering phenomenon that occurs during the activation process.[1]

Concerning the introduction of Zr into the three different types of LDHs studied, it should be pointed out that 95, 70, and 65% of the amounts of Zr in the solutions were introduced into the lamellar structures of Mg3Zr0.3, Ni3Zr0.3, and Zn3Zr0.3, respectively. This suggests that, when the size of the divalent cation decreases, the brucite-like layer accommodates increasing amounts of Zr. An opposite trend was actually expected, i.e., an easier substitution when the divalent cation was of a size similar to that of Zr^{4+}. Thus, the introduction of Zr probably accounted for the different behaviors of the solutions during precipitations performed at the same pH. However, in all cases, a lowering of the carbonate species symmetry appeared, as shown by IR spectroscopy. The formation of weakly bonded species responsible for the broadening of the second DTG peak toward lower temperatures also occurred. These changes resulted from the distortion of the layers and the heterogeneous distribution of charge upon the introduction of the large tetravalent Zr cations.

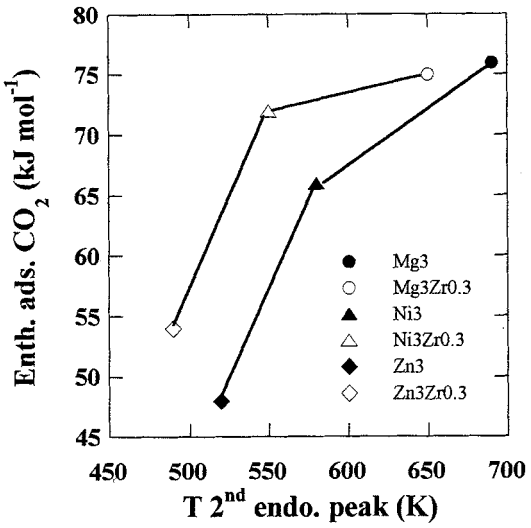

Figure 9. Correlation between the enthalpies of CO_2 adsorption and the temperature of the second peak in the heat flow profiles for the Zr-free (solid symbols) and Zr-containing (open symbols) samples.

The enthalpies of CO_2 adsorption and the temperatures of decarbonation, given by the second endotherm in the heat flow profile, increase in the same order for the three families of samples, as could be expected considering that both parameters are measures of the basic strength. These parameters are correlated in Figure 9 for Zr-free and Zr-containing LDH homologues with the composition $M(II)/Al/Zr = 3/0.7/0.3$. Because the basicities of different mixed oxides obtained from LDHs with similar M(II)/M(III) ratios are mainly dependent on the electronegativities of the components,[23] the order of basicity, Zn < Ni < Mg, is consistent with the expected results.

The lower basic strength of Zn-containing LDHs is otherwise confirmed by the large decrease in intensity of the carbonate IR bands after evacuation above 723 K. Considering the three families of samples, Figure 9 provides evidence that the introduction of Zr into the structure has opposite effects on the enthalpy of adsorption of CO_2 and on the decarbonation temperature of the LDH. The former increases, whereas the latter decreases. It is worth noting that CO_2 is adsorbed on the surfaces of the mixed oxides, whereas the decarbonation temperature concerns the lamellar structure; therefore, these evolutions show that the two types of structures behave differently upon addition of the tetravalent cation. Substitution of Zr for Al induces a lowering of the mean partial charge of the oxygen atoms despite their similar polarizing power. Therefore, the increase in basicity upon the introduction of Zr accounts for the different natures of the basic sites on the surfaces. A net surface segregation of Al in Mg(Al)O

(34) Roussel, H.; Briois, V.; Elkaim, E.; de Roy, A.; Besse, J. P. *J. Phys. Chem. B* **2000**, *104*, 5915.

mixed oxides has been demonstrated upon the calcination of the LDHs, as well as the formation of $Al^{3+}-O^{2-}$ and $Mg^{2+}-O^{2-}$ acid−base pair sites.[35−37] In Zr-containing samples, both the segregation of ZrO_2 and the formation of small amounts of $Zr^{4+}-O^{2-}$ pairs could account for the increase in basicity. ZrO_2 is less acidic than Al_2O_3, and O^{2-} sites in the vicinity of Zr^{4+} could be stronger anionic sites than those in the vicinity of Al^{3+}. In agreement with this proposition, the increase in basicity is indeed higher in Zn-containing mixed oxides in which the segregation of Zr appears to higher.

A higher basic strength of the decarbonated LDHs has also been identified by XPS through a comparison of the binding energies of the O(1s) lines, which are shifted by about 1 eV to lower values after calcination of the fresh samples, thus showing an increase in the negative charge on oxygen.[23] This effect could perhaps be enhanced by the introduction of tetravalent cations into the LDHs.

Concluding Remarks

Pure lamellar phases of M(II)/Al/Zr LDHs with M(II) = Mg, Ni, and Zn were prepared at pH 10 for a wide range of compositions but with a greater distortion of the layers as the amount of Zr increased. Indeed, the ability to accommodate Zr in the layers improved as the size of the divalent cation decreased. Zn-LDHs exhibited a peculiar behavior in the precipitation of lamellar phases having similar Al/(Zn + Al) or (Al + Zr)/(Zn + Al + Zr) ratios regardless of the compositions in solution, probably with the formation of an additional zinc hydroxycarbonate phase.

Calcination at 723 K led to the formation of mixed oxides whose cell parameters suggested higher segregation of Zr in Zn- than in Mg-containing materials. The latter mixed oxides were fully reconstructed in water at ambient temperature and atmospheric pressure. In contrast, a slight amount of ZnO-like phase remained in Zn-containing LDHs. The incorporation of Zr into the LDH lattice had a varying influence on the basicity of the lamellar and mixed oxide structures because of the polarizing power of the cation and the probable segregation of ZrO_2, respectively. This effect mostly influenced the basicity of the Zn-LDHs.

Acknowledgment. N. Das is thankful to Department of Science & Technology, Government of India, for a BOYCAST fellowship.

CM011125L

(35) Tichit, D.; Lhouty, M. H.; Guida, A.; Chiche, B. H.; Figueras, F.; Auroux, A.; Bartalini, D.; Garrone, E. *J. Catal.* **1995**, *151*, 50.
(36) Di Cosimo, J. I.; Diez, V. K.; Xu, M.; Iglesia, E.; Apesteguia, C. R. *J. Catal.* **1998**, *178*, 499.
(37) Prinetto, F.; Ghiotti, G.; Durand, R.; Tichit, D. *J. Phys. Chem. B* **2000**, *104*, 11117.